Advancements in X-Ray Diffraction and X-Ray Free-Electron Lasers

Simon Lavoie[1]

[1] *Department of Physics, McGill University*

(Dated: February 2025)

Due to their nanometer-scale wavelengths, X-rays are well-suited for probing atomic-scale structures. This paper discusses advancements in X-ray diffraction (XRD) and the impact of improved X-ray sources, including synchrotrons and X-ray free-electron lasers (XFELs), on structural studies in physics, chemistry, and biology. Topics include the historical context of XRD, Bragg's law, experimental techniques, and modern computational analysis methods such as Fourier transform analysis and Rietveld refinement. Challenges in data acquisition and recent technological developments will also be explored.

CONTENTS

I. INTRODUCTION

X-ray diffraction (XRD) has been instrumental in elucidating atomic structures since its experimental validation in 1912. With the advent of synchrotrons and XFELs, the technique has undergone significant refinement, enabling time-resolved imaging and single-particle studies.

II. THEORETICAL FRAMEWORK

A. Bragg's Law

Shortly after Röntgen's discovery of X-rays, Max von Laue suggested that X-rays could be diffracted by crystals, which Friedrich and Knipping experimentally confirmed in 1912. The underlying principle was formalized by W. H. Bragg and W. L. Bragg through:

$$2d\sin\theta = n\lambda, \tag{1}$$

where d is the regular spacing between the atoms, θ the angle of incidence, n an integer, and λ the X-ray wavelength [1]. As an X-ray beam incident upon a crystal interacts with the electrons of the lattice's atoms, it is scattered spherically in all directions. The scattered X-rays from adjacent atoms interfere constructively and destructively, producing a diffracted beam. The condition for constructive interference is given by Eq. 1. That is, when the path difference between two adjacent rays ($2d\sin\theta$) is an integer multiple of the wavelength, the waves will superimpose in phase, leading to peaks in the diffracted intensity. This phenomenon is illustrated in Fig. 2.

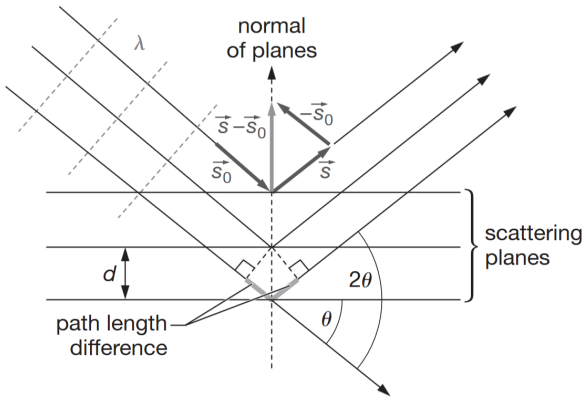

FIG. 1. Geometry of a beam with angle of incidence θ approaching from the left into a symmetrical arrangement of atoms forming the lattice of a crystal [2].

B. The Structure of Crystals

The theory of crystals and how they are structured is essential to understanding X-ray diffraction. Crystals are regular arrangements of atoms in three dimensions, exhibiting translational symmetry. The discrete points at which the atoms of a crystal are located can be described mathematically by

$$\mathbf{R} = n_1\mathbf{a}_1 + n_2\mathbf{a}_2 + n_3\mathbf{a}_3, \tag{2}$$

where $\mathbf{a}_1$, $\mathbf{a}_2$, and $\mathbf{a}_3$ are the primitive vectors of the lattice and n_1, n_2, and n_3 are integers. This infinite set of points defined by Eq. 2 forms a Bravais lattice, and the parallelepiped comprised of these primitive vectors is called the unit cell. The constraint that crystals exhibit translational symmetry and repeat periodically in space leads to the classification of Bravais lattices into 14 distinct types [4]. These lattices can be further categorized into seven crystal systems based on the symmetry of the unit cell. The seven crystal systems are cubic, tetragonal, orthorhombic, hexagonal, rhombohedral,

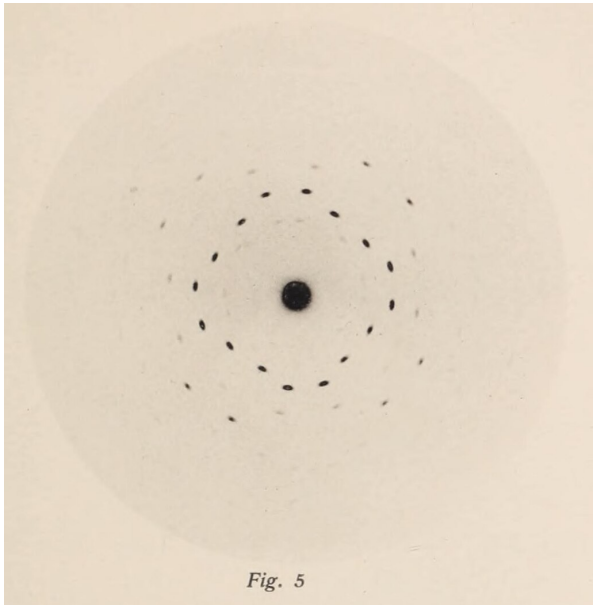

FIG. 2. X-ray diffraction pattern of a copper sulfate crystal from Friedrich and Knipping's 1912 paper [3].

monoclinic, and triclinic. The concept of a reciprocal lattice, which is especially useful in X-ray diffraction, is defined as the set of all wave vectors $\mathbf{k}$ that yield plane waves with the periodicity of the Bravais lattice [5]. The reciprocal lattice itself is spanned by three primitive vectors $\mathbf{b}_1$, $\mathbf{b}_2$, and $\mathbf{b}_3$ which can be generated from the lattice's primitive vectors via:

$$\mathbf{b_i} = 2\pi \frac{\mathbf{a}_j \times \mathbf{a}_k}{\mathbf{a_i} \cdot (\mathbf{a}_j \times \mathbf{a}_k)}, \tag{3}$$

For any cyclic permutation of $i, j, k = 1, 2, 3$. The triple scalar product in the denominator is physically interpreted as the volume of the unit cell. The factor of 2π ensures that the reciprocal lattice vectors are properly scaled so that plane waves match the periodicity of the crystal. The reciprocal lattice vector is then defined as:

$$\mathbf{G} = h\mathbf{b}_1 + k\mathbf{b}_2 + l\mathbf{b}_3, \tag{4}$$

where h, k, and l are integers, commonly known as the Miller indices. $\mathbf{G}$ is perpendicular to the family of planes indexed by (hkl), these being the planes that diffract the incident X-rays. The inter-planar spacing d for a cubic crystal, for example, is given by:

$$d = \frac{a}{\sqrt{h^2 + k^2 + l^2}}, \tag{5}$$

where a is the lattice parameter, which represents the length of the unit cell's sides. For a cubic crystal, we have $a = |\mathbf{a}_1| = |\mathbf{a}_2| = |\mathbf{a}_3|$. For other crystal systems (e.g., tetragonal, orthorhombic), the interplanar spacing depends on a more general relation between the Miller indices, the lattice parameters, and the metric tensor of the crystal system [6].

III. EXPERIMENTAL METHODS

A. X-ray Sources

Modern XRD experiments use high-brilliance sources such as synchrotrons and XFELs to generate X-rays. X-ray sources are characterised by their brilliance, which is the ratio of the intensity (photons per second) of the beam to its spatial coherence, which is proportional to the product of the size (m^2), bandwidth and angular divergence of the beam. The difference in brilliance between XFELs and synchrotrons is drastic, with XFELs exhibiting higher brilliance by several orders of magnitude due to their high peak power and short pulse duration [7]. A comparison of the avberage brilliance of XFEL and synchrotron facilities is shown in Fig. 3.

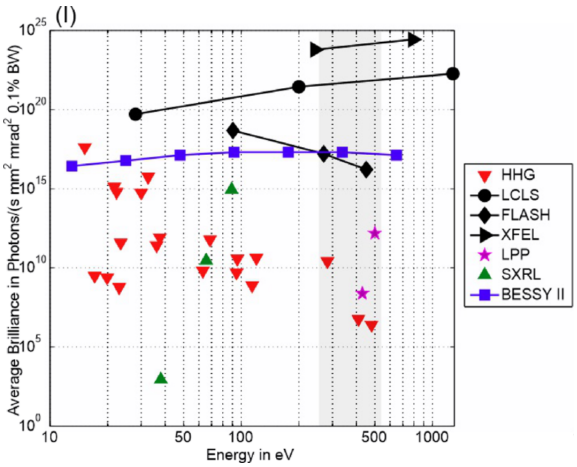

FIG. 3. Comparison of brilliance versus energy between X-ray user facilities on a log-log scale. [8]. LCLS, FLASH and European XFEL (simply labelled XFEL) are XFELs, BESSY II is a synchrotron, and the others are High Harmonic Generation (HHG), Soft X-Ray Laser (SXRL) and Laser Produced Plasma (LPP) facilities.

These sources operate in a similar manner, accelerating electrons to relativistic speeds before channeling them through undulators to produce X-rays. Undulators, as can be seen in fig 4, are arrays of magnets of periodically alternating polarities. As an electron enters this array at velocity $\mathbf{u} \approx c$, it undergoes synchrotron radiation due to the acceleration caused by the sinusoidal magnetic field. In the electron's centre of mass frame, where the undulator approaches at speed $-\mathbf{u}$, the undulator transverse $\mathbf{B}$ field becomes the combination of a transverse $\mathbf{B}$ field

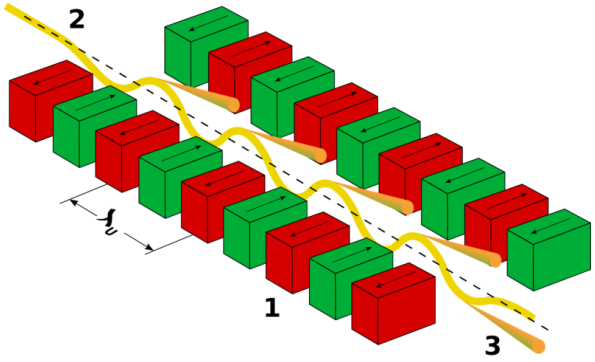

FIG. 4. Undulator schematic. Pictured are (1) two rows of adjacent magnets of opposing polarities with spacing $\lambda_u/2$, (2) incident beam of electrons and (3) emitted radiation.

and a transverse $\mathbf{E}$ field via the Lorentz boosts:

$$\mathbf{E}'_{\parallel} = \mathbf{E}_{\parallel}, \quad \mathbf{B}'_{\parallel} = \mathbf{B}_{\parallel} \tag{6}$$

$$\mathbf{E}'_{\perp} = \gamma(\mathbf{E}_{\perp} - u\mathbf{B}_{\perp}) \tag{7}$$

$$\mathbf{B}'_{\perp} = \gamma\left(\mathbf{B}_{\perp} + \frac{u}{c^2}\mathbf{E}_{\perp}\right) \tag{8}$$

where $\gamma = \frac{1}{\sqrt{1-v^2/c^2}}$. Since the undulator field in the lab frame is purely magnetic ($\mathbf{E} = 0$), the transverse field in the electron's rest frame simplifies to $\mathbf{E}'_{\perp} = -\gamma u\mathbf{B}_{\perp}$. In essence, the system looks like an electromagnetic wave approaching the electron, which in-turn causes the electron to radiate photons of equal wavelength. This wavelength is given by the undulator period λ_u corrected for length contractions ($\lambda = \lambda_u/\gamma$). However, the transverse velocity $\mathbf{u}_{\perp}$ induced by the undulator field slightly modifies the electron's velocity components. Since the Lorentz force cannot perform work, the total kinetic energy remains unchanged, but $\mathbf{u}_{\perp}$ reduces the electron's longitudinal velocity to values below $\mathbf{u}$. It can therefore be shown that the wavelength measured in the lab frame becomes

$$\lambda = \frac{\lambda_u}{2\gamma^2}\left(1 + \frac{K^2}{2}\right) \tag{9}$$

where,

$$K = \frac{eB_0\lambda_u}{2\pi m_e c}. \tag{10}$$

is known as the deflection parameter and is equal to the maximum angular excursion of the beam in units of $1/\gamma$. Any device having $K < 1$ is known as an undulator, while one with $K \gg 1$ is called a wiggler [**?**]. This result is handy as it entails that the emitted wavelength of an XFEL may be tuned by adjusting the magnetic field strength. It also reveals how much energy is required to accelerate electrons to sufficient speeds such that X-rays are emitted.

In reality, XFELs emit light with a bandwidth $\Delta\lambda$ centered around the wavelength given by equation 9. This is due the fact that each of the N_u oscillations of the electron's sinusoidal motion contributes a wave packet of finite duration. The total physical length of the resulting wave train is thus $L_t = N_u\lambda_u$, which leads to a wave train duration of $T_t \approx L_t/c = N_u\lambda_u/c$. Since the Fourier transform of a finite-length wave scales as $1/T_t$, the spectral width becomes

$$\frac{\Delta\lambda}{\lambda} = \frac{1}{N_u}, \tag{11}$$

or $1/mN_u$ for the m^{th} harmonic [**?**].

B. Microbunching and Self-Amplified Spontaneous Emission (SASE)

In reality, it is not a single electron that is accelerated into the undulator, but groups of them called bunches.

IV. DATA ACQUISITION AND ANALYSIS

Techniques such as Fourier transform analysis and Rietveld refinement allow for precise structural determination.

V. CHALLENGES AND FUTURE PROSPECTS

High facility costs and limited access remain key limitations. Advances in AI-driven data processing and compact XFELs promise to expand accessibility.

[1] W. H. Bragg and W. L. Bragg, Proceedings of the Royal Society of London. Series A, Containing Papers of a Mathematical and Physical Character **88**, 428 (1913).

[2] G. S. Girolami, Acta crystallographica. Section A, Foundations and advances **72 Pt 1**, 168 (2016).

[3] Königlich Bayerische Akademie der Wissenschaften. Mathematisch-Physikalische Klasse, Sitzungsberichte der Mathematisch-Physikalischen Classe **1912** (1912), available from the American Museum of Natural History Library.

[4] M. Pitteri and G. Zanzotto, Acta Crystallographica Section A - ACTA CRYSTALLOGR A **52**, 830 (1996).

[5] N. Ashcroft and N. Mermin, *Solid State Physics* (Saunders College Publishing, Philadelphia, 1976) available at: https://archive.org/details/AshcroftSolidState.

[6] Y. Liu, Y. Liu, and M. G. B. Drew, SN Applied Sciences **2**, 755 (2020).

[7] F. L. Baillet, M. A. Carpenter, and R. J. Angel, Reviews in Mineralogy and Geochemistry **78**, 1 (2014).

[8] T. Helk, M. Zuerch, and C. Spielmann, Structural Dynamics **6**, 010902 (2019).